

Analysis of Periodic Errors for Synthesized-Reference-Wave Holography

Jan PIDANIC, Vladimir SCHEJBAL, Dusan CERMAK

University of Pardubice, Jan Perner Transport Faculty, Studentska 95, 53210 Pardubice, Czech Republic

jan.pidanic@upce.cz, vladimir.schejbal@upce.cz, dusan.cermak@upce.cz

Abstract. *Synthesized-reference-wave holographic techniques offer relatively simple and cost-effective measurement of antenna radiation characteristics and reconstruction of complex aperture fields using near-field intensity-pattern measurement. These methods allow utilization of advantages of methods for probe compensations for amplitude and phasing near-field measurements for the planar and cylindrical scanning including accuracy analyses. The paper analyzes periodic errors, which can be created during scanning, using both theoretical results and numerical simulations.*

Keywords

Periodic errors, numerical simulations, accuracy analyses, near-field sampling, holography.

1. Introduction

Near-field (NF) measurements provide a fast and accurate method of determining the antenna gain, pattern, polarization, beam pointing etc. Near-field antenna measurement methods, in contrast to conventional far-field methods, make use of a measuring probe in the radiating near-field region of the antenna under test (AUT). The far-field radiation pattern of the AUT must then be indirectly computed from the measurements made in a near-field region. Several methods for near-field antenna measurements have been described [1]–[23].

The synthesized-reference-wave holography has been analyzed in [10]–[18], where several aspects have been thoroughly analyzed such as description of holographic near-field measurements using probe compensations for planar and cylindrical scanning shown in Fig. 1, which can be advantageously used for fan beam antennas [24]–[27], comparison of holographic near-field and far-field measurements with and without probe compensations and accuracy analyses using mathematical models considering random processes with correlation intervals, numerical simulations considering random errors as well as deterministic errors and processing of measurement statistics.

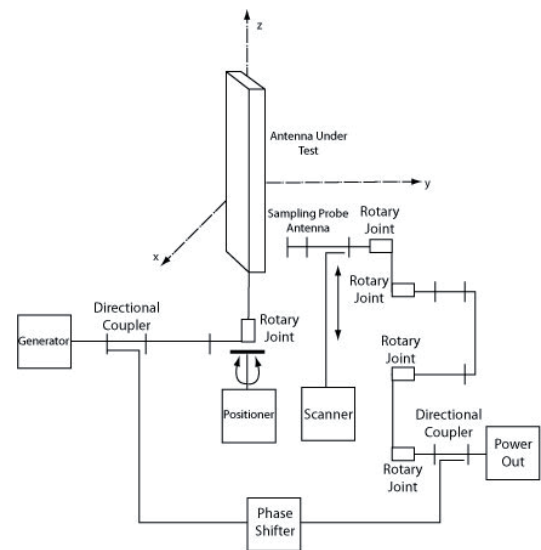


Fig. 1. Antenna cylindrical scanning using synthesized-reference-wave holography.

The synthesized-reference-wave holography allows employing advantages of methods for probe compensations for amplitude and phase near-field measurements for the planar and cylindrical scanning including accuracy analyses [1]–[7], which should be slightly modified. The NIST 18 term error model can be applied [4]–[7]. If sample spacing and computer accuracy are adequate, aliasing and computational errors would be negligible compared to the experimental errors. Importance of the various near-field measurement errors depends on the antenna under test, the frequency of operation, the measurement facility, and the probe but the results show that finite scan area, z -position of the probe for planar scanning, receiver nonlinearities in measuring the near-field amplitude, and sometimes, multiple reflections are usually the most important. The accuracy analyses using mathematical models considering random processes with correlation intervals, processing of measurement statistics and numerical simulations considering random errors as well as deterministic errors have been done [10], [11], [13], [14], [15], [17]. The given analyses correspond to measurements and/or numerical simulations.

This paper analyzes periodic errors, which can be created during scanning. It offers new more general

numerical simulations (in comparison with [16], [17]) and gives better understanding of the periodic error effects.

2. Analysis of Periodic Errors

The synthesized-reference-wave holographic techniques could be used for both planar and cylindrical scanning using probe compensations and polarization effects and therefore the NIST 18 term error model can be applied [4]-[7]. The fundamental difference is the utilization of the synthesized-reference-wave, which is only used for one axis regardless of planar or cylindrical scanning. That is comprehensively explained [11], [16]. Therefore, it is possible to consider one-dimensional scanning (along the x axis), and a synthesized reference signal with a linear phase change Ce^{-jax} (which simulates a plane wave propagating in the x direction with wave-number a), the following equation for the output signal (formed by the sampled near field, $E(x)$, and the synthesized reference signal, Ce^{-jax}) can be obtained [16]:

$$v(x) = |E(x) + Ce^{-jax}|^2 = |E(x)|^2 + |C|^2 + C^*E(x)e^{jax} + CE^*(x)e^{-jax} \tag{1}$$

The Fourier transform of (1), i.e., the complex plane-wave spectrum (PWS) with spatial frequency k_x , is

$$F[v(x)] = \frac{1}{\sqrt{2\pi}} \int_{-\infty}^{\infty} [|E(x)|^2 + |C|^2 + C^*E(x)e^{jax} + CE^*(x)e^{-jax}] e^{-jk_x x} dx \tag{2}$$

This can be simplified for $|k_x| < k_1$, using a suitable constant a . Multiplying by e^{-jax} corresponds to a shift. If it is known that $F[E(x)] = 0$ for $|k_x| \geq k_2$ and $F[|E(x)|^2] = 0$ for $|k_x| \geq k_3$, then

$$F[v(x)e^{-jax}] = F[C^*E(x)] \tag{3}$$

for $|k_x| < k_1$, $2a > k_1 + k_2$, $a > k_1 + k_3$ as the other terms are equal to zero for $|k_x| < k_1$. The PWS can be shown to be band-limited [1]. According to Riemann-Lebesgue lemma if n of the derivatives of $E(x)$ exist, then $F[E(x)]$ vanishes faster than n -th power of $1/k_x$, therefore the PWS becomes negligible beyond the k limit, and $k_1 = k_2 = k_3 > k$ can be chosen.

If the sample spacing $\Delta x \leq \lambda/6$ and $a\Delta x = 2\pi/3$, then space period is $N\Delta k_x = 2\pi/\Delta x \geq 12\pi/\lambda$, $a \geq 4\pi/\lambda$ and assumptions of (3) are clearly fulfilled. The spatial frequencies are shown in Figs. 2 – 12 for $k_x = 2\pi/\lambda, 4\pi/\lambda, 8\pi/\lambda$ and $10\pi/\lambda$ (due to fact that FFT is periodical with period $12\pi/\lambda$ the value of $10\pi/\lambda$ corresponds to the value of $-2\pi/\lambda$). The main lobes of PWS, which correspond to $E^*(x)$ and $|E(x)|^2$ occur at $4\pi/\lambda$ and $8\pi/\lambda$, respectively and they are in invisible region (complex space) because the visible region is between $-2\pi/\lambda$ and $2\pi/\lambda$ with the main lobe of PWS, which corresponds to $E(x)$.

The periodic errors can be created during scanning. The phase shifters do not change phases in the arbitrary range but for interval $\langle 0, 2\pi \rangle$, only. That means the values $\Phi - 2m\pi$ are only set, where m is the integer, instead of Φ . With a phase increment of $2\pi/3$, the phase state repeated every third line. In practice, this meant that the phase-shifter settings only needed to be changed on three occasions throughout the overall scan (data can be taken for line 1, line 4, line 7, etc. for zero shifter setting, for line 2, line 5, line 8, etc. for $2\pi/3$ shifter setting and for line 3, line 6, line 9, etc. for $4\pi/3$ shifter setting). Eq. (3) has been thoroughly explained and verified by both several experiments and numerical simulations [10]-[18]. That means the phase increment of $2\pi/3$ should be only analyzed. The modification of the synthetic-plane-wave-based holographic technique for determining radiation patterns and aperture fields [28] uses quite different procedure and therefore it is not analyzed here.

The phase periodic errors have been analyzed by several authors such as [22]. If the errors are $\Delta_S = \delta \sin \Phi$, where δ is the error amplitude, $\Phi = -ax$ are the required phase values, then the following equation is valid for $|k_x| < k_1$ interval [16]:

$$F[v_s(x_1)e^{-j\alpha x_1}] = F[C^*E(x_1)] + \frac{\delta}{2} F[CE^*(x_1)e^{-3j\alpha x_1}] \tag{4}$$

as the other terms are equal to zero for $|k_x| < k_1$ interval. The span of space period $N\Delta k_l$ determines, if the last term would appear in the $|k_x| < k_1$ interval.

3. Numerical Simulations

A typical near-field distribution is one where the phase varies quickly at the edge and the amplitude is small. Therefore, the input sequence, i.e., the near-field distribution, $E(i)$, can be considered to be of the following form [15]:

$$E(i) = \sin^\alpha(\pi i / 64) \exp(j((i - 32) / 32)^2 \beta + j\pi m / 3) \tag{5}$$

where $i = 1, 2, \dots, 64$, $m = i$ for $i = 1, 2, \dots, 11$, $m = 0$ for $i = 12, 13, \dots, 53$ and $m = -i$ for $i = 54, 55, \dots, 64$ (that represents the phase variations according to numerous experiments and numerical simulations such as [5], [11], [14], [16], [17], when the distance between aperture and scanning axis is very small, otherwise the quadratic phase with a larger β should be added), α and β are constants. Numerical simulations can be done using (1) and (3)

$$F[v(i)e^{-j12\pi/3}] / C^* = F[E(i)] \tag{6}$$

for a region of space where the electromagnetic field contains no evanescent waves (the far-field of an antenna). Considering this region the near-field distribution $E(i)$ could be obtained by inverse Fourier transform. Some of the numerical simulation results are shown for $\beta = \pi/4$ in Fig. 2 – 10 and $\beta = 3\pi/4$ in Fig. 11 and 12.

To increase the resolution (i.e., decrease the angular separation between far-field points), it is possible to add zeros to the near-field data (zero-filling). The input sequence $E(l)$ according to (5) was added with zeros and changed numbering (therefore l instead of i is used).

The synthesized reference signal with a linear phase change $Ce^{-j\alpha x}$ is changed. The amplitude periodic error is considered as

$$\Delta_l = e \text{ mod}(l,3) \tag{7}$$

For numerical simulations, various e could be chosen. The periodic error $e = -\pi/30$ is used in Fig. 2 – 5 and the periodic error $e = \pi/30$ is used in Fig. 6 – 9. The far-field amplitudes obtained by FFT using synthesized reference-wave holography are shown by a solid line, direct near-field measurements are shown by a dashed line and results including measurement errors with the periodic error $e = -\pi/30$ are shown by a dotted line for $\alpha = 3$ in Fig. 2.

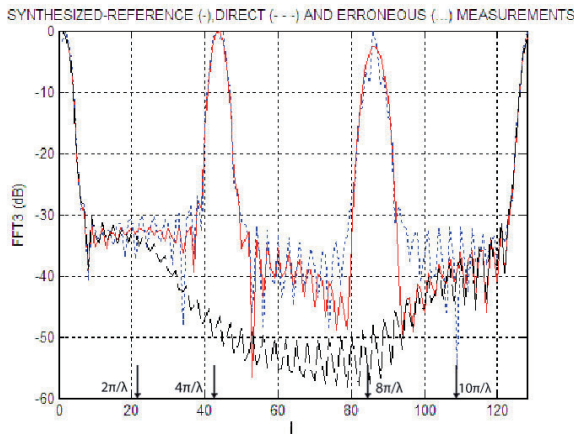


Fig. 2. Far-field amplitudes obtained by synthesized reference-wave holography (solid line), direct near-field measurements (dashed line) and results including measurement errors with $e = -\pi/30$ for $\alpha = 3$ and $\beta = \pi/4$.

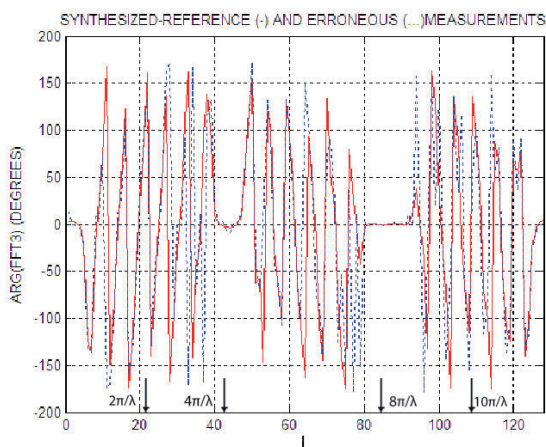


Fig. 3. Far-field phases obtained by synthesized reference-wave holography (solid line) and results including measurement errors with $e = -\pi/30$ for $\alpha = 3$ and $\beta = \pi/4$.

The detailed comparison of the synthesized reference-wave holography and direct near-field measurements including random processes with correlation intervals, processing of measurement statistics and numerical simulations considering random errors as well as deterministic errors have been done in [10]-[17] and therefore it is not accomplished here. The far-field phases obtained by FFT using synthesized reference-wave holography are shown by a solid line and results including measurement errors with the periodic error $e = -\pi/30$ are shown by a dotted line for $\alpha = 3$ in Fig. 3.

The far-field amplitudes obtained by FFT using synthesized reference-wave holography are shown by a solid line and results including measurement errors with the periodic error $e = -\pi/30$ are shown by a dotted line for $\alpha = 4$ in Fig. 4. The far-field phases obtained by FFT using synthesized reference-wave holography are shown by a solid line and results including measurement errors with the periodic error $e = -\pi/30$ are shown by a dotted line for $\alpha = 4$ in Fig. 5.

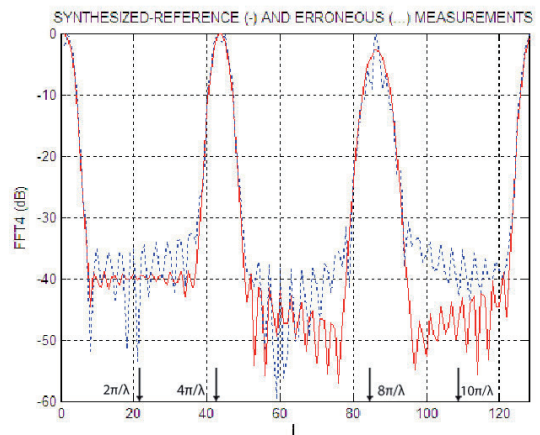


Fig. 4. Far-field amplitudes obtained by synthesized reference-wave holography (solid line) and results including measurement errors with $e = -\pi/30$ for $\alpha = 4$ and $\beta = \pi/4$.

The far-field amplitudes obtained by FFT using synthesized reference-wave holography are shown by a solid line and results including measurement errors with the periodic error $e = \pi/30$ are shown by a dotted line for $\alpha = 3$ in Fig. 6. The far-field phases obtained by FFT using synthesized reference-wave holography are shown by a solid line and results including measurement errors with the periodic error $e = \pi/30$ are shown by a dotted line for $\alpha = 3$ in Fig. 7.

The far-field amplitudes obtained by FFT using synthesized reference-wave holography are shown by a solid line and results including measurement errors with the periodic error $e = \pi/30$ are shown by a dotted line for $\alpha = 4$ in Fig. 8. The far-field phases obtained by FFT using synthesized reference-wave holography are shown by a solid line and results including measurement errors with the periodic error $e = \pi/30$ are shown by a dotted line for $\alpha = 4$ in Fig. 9.

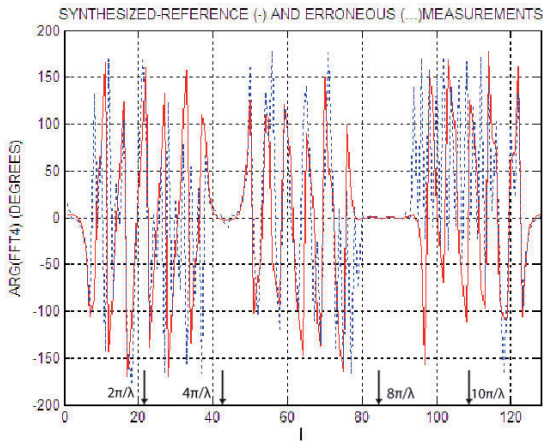


Fig. 5. Far-field phases obtained by synthesized reference-wave holography (solid line) and results including measurement errors with $e = -\pi/30$ for $\alpha = 4$ and $\beta = \pi/4$.

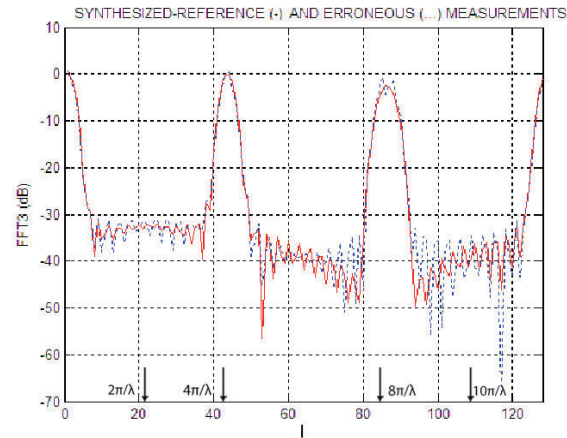


Fig. 6. Far-field amplitudes obtained by synthesized reference-wave holography (solid line) and results including measurement errors with $e = \pi/30$ for $\alpha = 3$ and $\beta = \pi/4$.

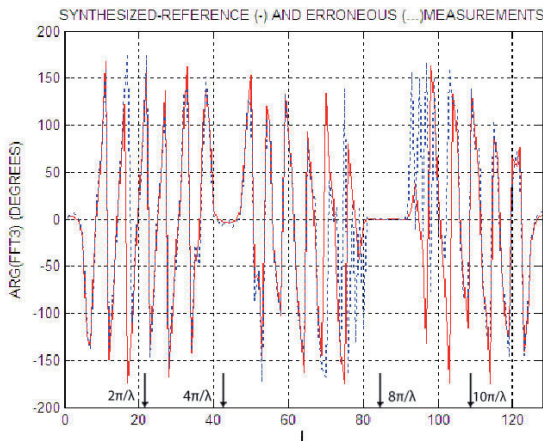


Fig. 7. Far-field phases obtained by synthesized reference-wave holography (solid line) and results including measurement errors with $e = \pi/30$ for $\alpha = 3$ and $\beta = \pi/4$.

The numerical simulations of far-field amplitudes obtained by FFT using synthesized reference-wave holography are shown by a solid line and the difference of synthesized-reference and results including periodic

phase measurement errors according to (4) with errors $\Delta_S = \delta \sin \Phi$, where $\Phi = -ax$ and $\delta = \pi/30$, with estimations according to (4) are shown by a dotted line for $\alpha = 3$ and $\beta = \pi/4$ in Fig. 10. When a phase periodic error

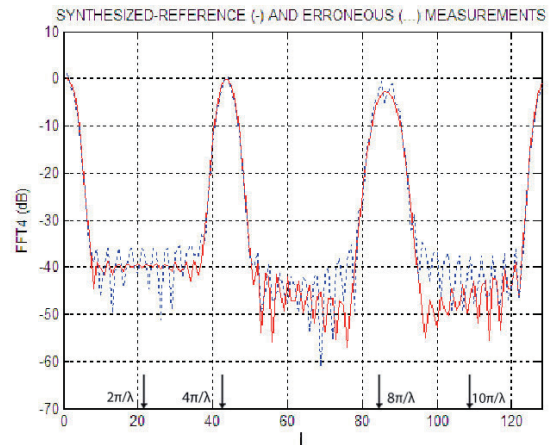


Fig. 8. Far-field amplitudes obtained by synthesized reference-wave holography (solid line) and results including measurement errors with $e = \pi/30$ for $\alpha = 4$ and $\beta = \pi/4$.

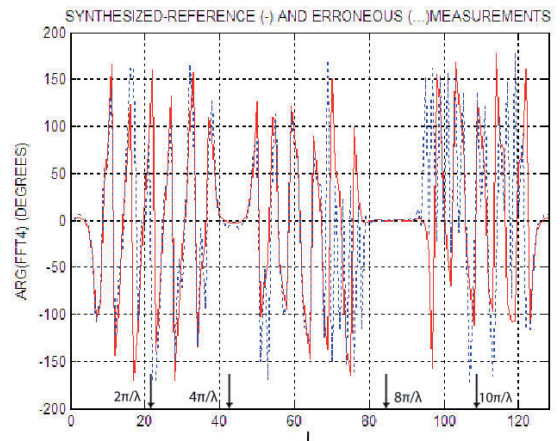


Fig. 9. Far-field phases obtained by synthesized reference-wave holography (solid line) and results including measurement errors with $e = \pi/30$ for $\alpha = 4$ and $\beta = \pi/4$.

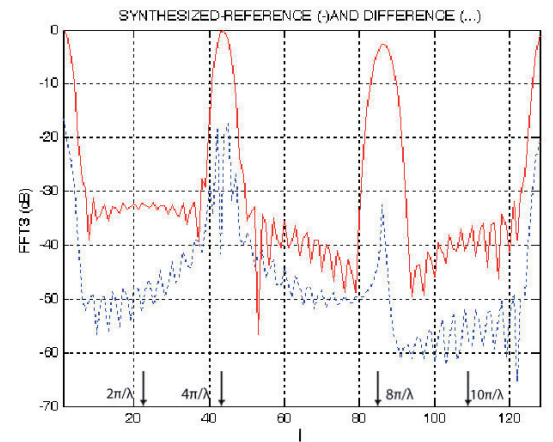


Fig. 10. Far-field amplitudes obtained by synthesized reference-wave holography (solid line) and difference of synthesized-reference and results including periodic measurements errors with $\delta = \pi/30$ for $\alpha = 3$ and $\beta = \pi/4$.

is considered with the same dependence as amplitude periodic error, given by (7), the results of numerical simulations are very similar as $\exp(j\alpha) \approx 1 + j\alpha$ for $|\alpha| \ll 1$ and therefore they are not shown. Similarly, the comparison of numerical simulations for phase and amplitude measurement errors with results according to (4) demonstrates that results are similar and therefore they are not shown.

To analyze the affect of distance between aperture and scanning axis, a larger quadratic phase ($\beta = 3\pi/4$) is used in Fig. 11 and 12. The comparison of Fig. 2 and 11 and 3 and 12 reveals that the effect of $\beta = 3\pi/4$ on the results could be very small (especially for greater antennas, where far sidelobes are very low).

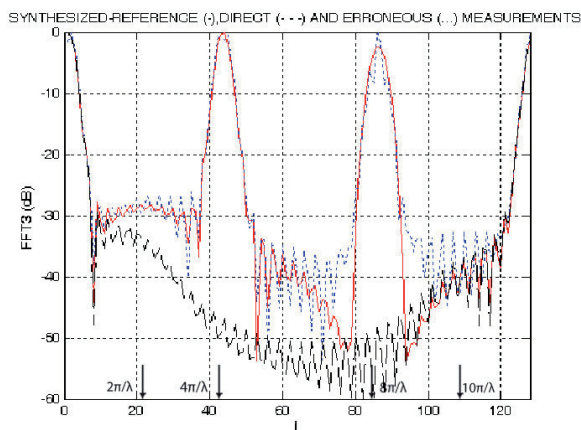


Fig. 11. Far-field amplitudes obtained by synthesized reference-wave holography (solid line), direct near-field measurements (dashed line) and results including measurement errors with $e = -\pi/30$ for $\alpha = 3$ and $\beta = 3\pi/4$.

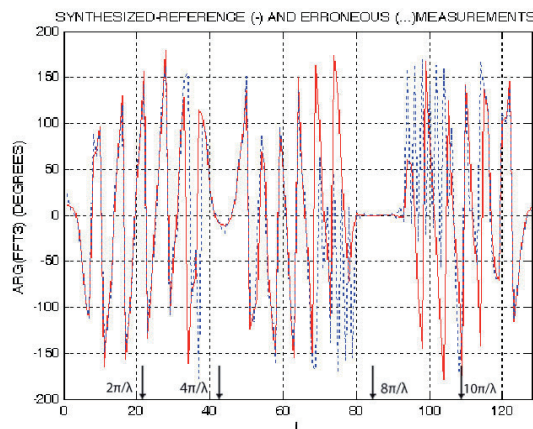


Fig. 12. Far-field phases obtained by synthesized reference-wave holography (solid line) and results including measurement errors with $e = -\pi/30$ for $\alpha = 3$ and $\beta = 3\pi/4$.

It is clear that the amplitude periodic errors of reference signals could distort not only amplitude of reference signal $Ce^{-j\alpha x}$ but also the phase of resulting reference signal. Moreover, the combination of amplitude and phase error could be expected and therefore periodic errors $e = -\pi/30$ and $e = \pi/30$ have been considered. Consequently, a dependence of resulting signal (1) could be very complicated. It can be seen that the periodic

error $e = -\pi/30$ (shown in Fig. 2 – 5) creates higher sidelobes than the periodic error $e = \pi/30$ (shown in Fig. 6 – 9). The parameter α affects sidelobe level (compare Fig. 2 and 6 and Fig. 5 and 7), and therefore the periodic error e creates much higher sidelobes for lower sidelobe levels ($\alpha = 4$, see Fig. 4 and 8).

A mitigation of periodic errors could be done using non-uniformly spaced samples with a special interpolation technique for the reconstruction of uniformly spaced [23] samples from non-uniformly spaced ones.

4. Conclusions

Synthesized-reference-wave holographic techniques, which offer relatively simple and cost-effective measurement of antenna radiation characteristics and reconstruction of complex aperture fields using near-field intensity-pattern, allows employing advantages of methods for probe compensations for amplitude and phase near-field measurements for the planar and cylindrical scanning including accuracy analyses. Importance of the various near-field measurement errors depends on the antenna under test, the frequency of operation, the measurement facility, and the probe. However, the results show that finite scan area, z -position of the probe for planar scanning, receiver nonlinearities in measuring the near-field amplitude, and sometimes, multiple reflections are usually the most important.

This paper analyzes periodic errors due to the synthesized-reference-wave holographic technique, which can be created during scanning, using both theoretical results and numerical simulations. It offers new more general numerical simulations and gives better understanding of the periodic error effects. The far-field phases are affected similarly.

The parameter α affects sidelobe level (compare Fig. 2 and 6 and Fig. 5 and 7), and therefore the periodic error e creates much higher sidelobes for lower sidelobe levels ($\alpha = 4$, see Fig. 4 and 8). The comparison of approximate error estimation (4) with numerical simulations shown in Fig. 10 elucidates the nature of periodical errors created during scanning as the phase shifters do not change phases in the arbitrary range but for interval $\langle 0, 2\pi \rangle$ only. The comparison of Fig. 2 and 11 and 3 and 12 reveals that the effect of β on the results could be very small. A mitigation of periodic errors could be done using non-uniformly spaced samples.

Acknowledgements

The paper is supported by the Czech National Institutional Research “Theory of Transport System” No. MSM 0021627505. The authors are thankful to the reviewers, whose suggestions helped a lot in improving the article.

References

- [1] YAGHJIAN, A. D. An overview of near-field antenna measurements. *IEEE Trans. Antennas and Propagation*, 1986, vol. 34, no. 1, pp. 30 - 45.
- [2] SLATER, D. Near-field test facility design. In *Antenna Measurement Techniques Association Conference*. 1985.
- [3] BUCCI, O. M., MIGLIORE, M. D. A new method for avoiding the truncation error in near-field antennas measurements. *IEEE Trans. Antennas & Propag.*, 2006, vol.54, no.10, p.2940-2952.
- [4] NEWELL, A. C. Error analysis techniques for planar near-field measurements. *IEEE Trans. Antennas and Propagation*, 1988, vol. 36, no. 6, pp. 754-768.
- [5] YAGHJIAN, A. D. *Upper-Bound Errors in Far-Field Antenna Parameters Determined From Planar Near-Field Measurements. Part 1: Analysis*. National Bureau of Standards Technical Note 667. Boulder, Oct. 1975.
- [6] NEWELL, A. C., STUBENRAUCH, C. F. Effect of random errors in planar near-field measurement. *IEEE Trans. Antennas and Propagation*, 1988, vol.36, no. 6, pp. 769 - 773.
- [7] NEWELL, A. C., LEE, D. Application of the NIST 18 term error model to cylindrical near-field antenna measurements. In *Antenna Measurement Techniques Association Conference*, Philadelphia, Oct. 2000.
- [8] BROCKETT, T., RAHMAT-SAMII, Y. A novel portable bipolar near-field measurement system for millimeter-wave antennas: construction, development, and verification. *IEEE Antennas & Propag. Magazine*, 2008, vol. 50, no. 5, pp. 121-130.
- [9] KAPLUN, I. V., KUROCHKIN, A. P. Analysis of random errors in holographic technique determination of directional antenna characteristics. *Radiotekhnika i Elektronika*, 1975, vol. XX, no. 10, pp. 2038-2045.
- [10] SCHEJBAL, V., HONIG, J. Holographic method of near-field antenna measurements. In *10th European Microwave Conference*, Warszawa (Poland), 1980, pp. 167 - 171.
- [11] SCHEJBAL, V. *Microwave Antenna Near-Field Measurements*. PhD thesis, SAV Bratislava (Slovakia), 1979, (in Czech).
- [12] SCHEJBAL, V., KOVARIK, V. Holography methods for antenna near-field measurement. *Tesla Electronics*, 1980, vol. 13, no. 2, pp. 35 - 39.
- [13] SCHEJBAL, V. Numerical simulation of near-field antenna measurement. *Tesla Electronics*, 1980, vol. 13, no. 3, p. 67- 72.
- [14] SCHEJBAL, V., KOVARIK, V. Accuracy of near-field antenna measurement using holography. *Tesla Electronics*, 1981, vol. 14, no. 2, pp. 48 - 52.
- [15] SCHEJBAL, V. Numerical simulations of problems occurring in near-field antenna measurements. In *7th Colloquium on Microwave Commun.* Budapest (Hungary), 1982, pp. 507 - 510.
- [16] SCHEJBAL, V., KOVARIK, V., CERMAK, D. Synthesized-reference-wave holography for determining antenna radiation characteristics. *IEEE Antennas and Propagation Magazine*, 2008, vol. 50, no. 5, pp. 71 - 83.
- [17] SCHEJBAL, V., PIDANIC, J., KOVARIK, V., CERMAK, D. Accuracy analyses of synthesized-reference-wave holography for determining antenna radiation characteristics. *IEEE Antennas & Propag. Magazine*, 2008, vol. 50, no. 6, pp. 89- 98.
- [18] SMITH, D., LEACH, M., ELSDON, M., FOTI, S. J. Indirect holographic techniques for determining antenna radiation characteristics and imaging aperture fields. *IEEE Antennas and Propagation Magazine*, 2007, vol. 49, no. 1, pp. 54 - 67.
- [19] COSTANZO, S., DI MASSA, G. Wideband phase retrieval technique from amplitude-only near-field data. *Radioengineering*, 2008, vol. 17, no. 4, pp. 8 - 12.
- [20] GUTERMAN, J., MOREIRA, A. A., PEIXEIRO, C., RAHMAT-SAMII, Y. User interaction with inverted-F antennas integrated into laptop PCMCIA cards. *Radioengineering*, 2008, vol. 17, no. 2, pp. 13 - 18.
- [21] PUSKELY, J., NOVACEK, Z. Application of the global optimization approaches to planar near-field antenna phaseless measurements. *Radioengineering*, 2009, vol. 18, no. 1, pp. 9-17.
- [22] BAHADORI, K., RAHMAT-SAMII, Y. Characterization of effects of periodic and aperiodic surface distortions on membrane reflector antennas. *IEEE Trans. Antennas and Propagation*, 2005, vol. 53, no. 9, pp. 2782 - 2791.
- [23] DEGHANIAN, V., OKHOVAT, V., HAKKAK, M. A new interpolation technique for the reconstruction of uniformly spaced samples from non-uniformly spaced ones in plane-rectangular near-field antenna measurements. In *PIER 72*, 47-59, 2007.
- [24] SILVER, S. *Microwave Antenna Theory and Design*. New York: McGraw-Hill, 1949.
- [25] PIDANIČ, J., ČERMÁK, D., SCHEJBAL, V. Gain estimation of doubly curved reflector antenna. *Radioengineering*. 2008, vol. 17, no. 3, p. 38 - 41.
- [26] SCHEJBAL, V. et al. Czech radar technology. *IEEE Trans. Aerospace & Electronics Systems*, 1994, vol. 30, no. 1, p. 2-17.
- [27] BEZOUSEK, P., SCHEJBAL, V. Radar technology in the Czech Republic. *IEEE Aerospace and Electronic Systems Magazine*, 2004, vol. 19, no. 8, p. 27-34.
- [28] LEACH, M. P., SMITH, D., SKOBELEV, S. P. A Modified holographic technique for planar near-field antenna measurements. *IEEE Trans. Antennas and Propagation*, 2008, vol. 56, no. 10, pp. 3342 - 3345.

About Authors

Jan PIDANIC (*1979) received his MS degree from the University of Pardubice in 2005. He has been with the University as a lecturer. He is interested in digital signal processing, radar system, passive coherent location and UWB propagation. He has published over 10 papers.

Vladimir SCHEJBAL graduated from the Czech Technical University, Prague in 1970. He received the PhD degree from the Slovak Academy of Science, Bratislava in 1980. He was with the Radio Research Inst. Opocinec, Antenna Dept. from 1969 to 1993. From 1983 to 1986, he was on a leave with the Higher Inst. of Electronics (Microwave Dept.) Beni Walid, Libya as a lecturer. He has been with the University of Pardubice since 1994, now as a full professor and a head of the department. He is interested in microwave antennas and propagation. He has published over 140 papers. He is a senior IEEE member.

Dusan CERMAK (*1974) received his MS degree from the Czech Technical University in Prague in 2003 and his PhD degree from the University of Pardubice in 2007. He has been with the University of Pardubice since 2003 as an assistant professor. He is interested in simulations, measurements, radar antennas and propagation of electromagnetic waves. He took participation in various grants and projects such as UWB Technology for Radars FT-TA2/030 and COST 280. He has published over 30 papers.